



HAL
open science

Relationship between both thickness and degree of crystallisation of BN interphases and the mechanical behaviour of SiC/SiC composites

Héloïse Delpouve, Gérald Camus, Stéphane Jouannigot, Bruno Humez, Hervé Plaisantin, Claudie Josse, Sylvain Jacques

► To cite this version:

Héloïse Delpouve, Gérald Camus, Stéphane Jouannigot, Bruno Humez, Hervé Plaisantin, et al.. Relationship between both thickness and degree of crystallisation of BN interphases and the mechanical behaviour of SiC/SiC composites. *Journal of Materials Science*, 2022, 2022, 10.1007/s10853-022-07753-0 . hal-03799207

HAL Id: hal-03799207

<https://hal.science/hal-03799207>

Submitted on 5 Oct 2022

HAL is a multi-disciplinary open access archive for the deposit and dissemination of scientific research documents, whether they are published or not. The documents may come from teaching and research institutions in France or abroad, or from public or private research centers.

L'archive ouverte pluridisciplinaire **HAL**, est destinée au dépôt et à la diffusion de documents scientifiques de niveau recherche, publiés ou non, émanant des établissements d'enseignement et de recherche français ou étrangers, des laboratoires publics ou privés.

Relationship between both thickness and degree of crystallisation of BN interphases and the mechanical behaviour of SiC/SiC composites

Héloïse DELPOUVE⁽¹⁾, Gérald CAMUS⁽¹⁾, Stéphane JOUANNIGOT⁽¹⁾, Bruno HUMEZ⁽¹⁾, Hervé PLAISANTIN⁽¹⁾, Claudie JOSSE⁽²⁾, Sylvain JACQUES^{(1)*}

⁽¹⁾ LCTS UMR 5801, CNRS - University of Bordeaux, 3 allée de la Boétie, 33600 Pessac, France

⁽²⁾ Centre de Microcaractérisation Raimond Castaing (UAR 3623), University of Toulouse, UPS, CNRS, INPT, INSA - Espace Clément Ader, 3 rue Caroline Aigle, 31400 Toulouse, France

*corresponding author. e-mail: jacques@lcts.u-bordeaux.fr

Abstract

SiC/BN/SiC-Si single-ply composites with Hi-Nicalon STM fibres were synthesised by chemical vapour infiltration and the liquid route. These are model composites representing the behaviour of industrial composites intended to be used as structural parts in the hot sections of aeronautical engines. Four interphases with two different degrees of crystallisation and, in each case, two different thicknesses were tested. The interfacial shear stress measured by fibre push-out test is significantly higher when the crystallisation degree of the BN interphase is low, yet in this case it decreases with the thickness of the interphase. This higher interfacial bonding is also associated, albeit less significantly, with better macromechanical properties as measured by tensile and shear tests. The cracks observed in the composite with different microscopy techniques are also less long and open. Depending on the interphases, the debonds are more or less pronounced and occur preferentially at different locations in the interfacial system.

Keywords

ceramic matrix composite; interphase; fibre push-out; FIB-SEM; TEM; In-plane shear tests

Introduction

The ceramic matrix composites (CMCs) consisting of a SiC-based matrix reinforced with SiC-based fibres are replacing the traditional superalloys used in the hot sections of aeronautical engines [1, 2]. All the CMCs are the subject of intense research aimed at improving the processes for their manufacture and their thermomechanical behaviour [3-5]. Their mechanical behaviour is rendered non-brittle by the presence of an interface coating placed between the fibres and the matrix called "interphase" [6]. Pyrocarbon is the common interphase material but because of its sensitivity to oxidation it may be replaced by turbostratic boron nitride which has sp^2 -hybridized form and layered structure similar to pyrocarbon.

It has been known for several decades that the structure of the interfacial system, particularly the thickness and microstructural organisation of the interphase, has an effect on the micro- and macro-mechanical properties of CMCs [6-11]. In the particular case of BN interphases, work on this effect has been carried out with the first generations of fibres from the Nippon Carbon company (Tokyo, Japan), namely Nicalon™ [12] and Hi-Nicalon™ [13]. However, the thermal instability of the fibres, the sizing residues or unexpected effects during thermochemical treatments leading to the formation of undesired phases at the interfaces (free carbon and silica) often prevented a clear conclusion on the influence of the interphase itself on the mechanical properties of the CMC. In the case of latest generation fibres, De Meyere *et al.* have also shown that the thickness of the BN interphase influences the interfacial properties measured from micro-mechanical push-out tests [14]. Fibre push-out tests provide a direct measure of the local fibre-matrix interfacial bond strength [15-17]. They are very useful and can be repeated on a large number of fibres in the same specimen for statistical purpose yet, they are only complementary to macro-scale tests which are the only ones able to determine the global mechanical behaviour of the composite.

The aim of this study is to establish the relationships between a BN interphase in terms of thickness and microstructure, on both micro- and macro-mechanical properties of SiC/SiC composites. In an industrial composite made by CVI (chemical vapour infiltration), a batch process derived from CVD (chemical vapour deposition), there are usually variations in interphase thickness due to gas infiltration gradients in the depth of the fibrous preform [18]. Furthermore, in woven preforms, the fibres in contact one with each other may locally prevent the growth of the interphase during its synthesis because of lack of space. However, in the present study we are interested in the effect of the average interphase thickness for which the differences were obtained intentionally by varying the synthesis time. The degree of crystallisation and structural organisation of a BN coating, on the other hand, depends largely on the synthesis temperature [19, 20]. Its effect on the mechanical properties of CMCs was therefore studied by modifying the CVI temperature. Minicomposites consisting of a single straight

fibre tow are often used as model composites to study mechanical properties and associated damage mechanisms because they are easier to produce than industrial parts and are idealized units of CMC [21, 22]. Yet, these minicomposites suffer from a major drawback: the morphology of the fibre bundles (in terms of shape, volume content of the various constituents and undulation) is somewhat distant from their reality inside a structure. Besides, it is only possible to perform an on-axis tensile test. That is why another type of model composite has been preferred in the present work. It consists of a single 2D woven SiC fibre ply [20]. The "single-ply" model composite thus allows a good compromise between rapid and easy laboratory preparation, homogeneity of infiltration and representativeness of the industrial composite. Fibre push-out tests were used to assess the micromechanical behaviour, while tensile and shear tests were used for the macro-mechanical behaviour. The damage morphologies (matrix cracking, debonding and crack deflection) were observed by microscopy to investigate the links between the behaviours at different scales.

Experimental procedure

Synthesis

The single-ply SiC/BN/SiC-Si composites used in this study were synthesised in the same way as those used in the study carried out by Plaisantin *et al.* [20]. They were composed of a single 2D 8-harness satin-weave SiC fibre cloth (Hi-Nicalon S from NGS Advanced Fibers Co., Ltd., total thickness ≈ 0.5 mm), a BN interphase and a matrix comprising both SiC obtained by the gaseous route as well as Si obtained by the liquid route. The fibres were desized during a process comprising an oxidation step followed by a treatment step with an acid to remove the silica layer formed during the oxidation step [23]. The BN and SiC coatings were infiltrated in a hot-wall CVI reactor working at low pressure. The fibrous cloth was maintained compressed in a graphite tooling. The BN interphases were infiltrated at two temperatures, 900 °C and 1200 °C, respectively, from NH_3 and BCl_3 , with H_2 as diluent gas. Infiltration times were adjusted to achieve either "thin" or "thick" interphases, i.e. aiming for target thicknesses of 200 nm and 500 nm respectively. The SiC matrix was then infiltrated at low pressure in the same CVD/CVI apparatus from a mixture of hydrogen and methyltrichlorosilane at a temperature of about 1000 °C. It is worth mentioning that the samples were not exposed to the ambient air between the infiltration of the BN interphase and the infiltration of the SiC matrix. The samples were then removed from the graphite tooling and liquid silicon was infiltrated into the remaining matrix porosity using a special apparatus at a temperature slightly above the melting point of silicon for 30 minutes.

In what follows, four interphases are named $9/t$, $9/T$, $12/t$ and $12/T$ for thin and thick interphases synthesised at 900 °C and thin and thick interphases synthesised at 1200 °C respectively. The thicknesses of the interphases were measured at tow edges from scanning electron microscope observations of cross-sections obtained after laser cutting, epoxy resin embedding and mechanical polishing. These measurements were carried out at the centre and at the two opposite edges of the useful area from which the homogeneous mechanical test specimens were obtained. They are given in Table 1. It should be noted that, while the variability of the measured thicknesses is reasonable for CMC interphases, it appears particularly high in the case of interphase $12/T$. This may reflect a more difficult infiltration of the BN interphase into the fibre cloth at high temperatures.

Table 1 Interphase thicknesses measured by SEM at tow edges in the useful area SiC/BN/SiC-Si composites

	BN interphase	$9/t$	$9/T$	$12/t$	$12/T$
	synthesis temperature (°C)	900	900	1200	1200
	target thickness (nm)	200	500	200	500
edge 1 of useful area	mean (nm)	186	443	197	665
	standard deviation (nm)	91	170	52	472
centre of useful area	mean (nm)	195	485	151	517
	standard deviation (nm)	56	213	66	354
edge 2 of useful area	mean (nm)	204	398	196	572
	standard deviation (nm)	74	175	51	297

The cross-sectional areas of the specimens as well as the proportions of the respective components were obtained by image analysis of the observations made with an optical microscope also after laser cutting, embedding in resin and mechanical polishing. For information and taking into account all the measurements, the average value of the cross-sectional areas is 2.9 mm² with a standard deviation of 0.4 mm². The average volume fractions are 40%, 47% and 13% for the fibres, CVI silicon carbide and MI silicon (with standard deviations of 4%, 7% and 5%) respectively.

Fibre push-out tests

The test specimens were prepared using metallographic techniques with anhydrous cutting and polishing lubricants. Pieces of a few millimeters in length were cut from the single-ply composites and sandwiched between a silicon wafer and a glass slide, then embedded in epoxy resin. Sections of this sandwich with a thickness of approximately 800 μm were cut out with a diamond wire saw (ESCIL Well 3032) and then thinned by mechanical polishing using a diamond size down to 0.5 μm (Buehler, MINIMET™ 1000) to reach a total specimen thickness of about 100 μm . This low thickness allows achieving complete debonding and fibre sliding during the push-out test [24] as it avoids both excessive wear effects, exaggerated shear stresses at the interface and the risk of fibre misalignment [14]. The push-out tests were carried out with a nanoindenter (Micro Materials Ltd, NanoTest NTX) equipped with a flattened conical diamond tip of 5.5 μm diameter. This fulfils the optimal ratio of 1:2 for the tip:fibre diameter found by De Meyere *et al.* to properly perform push-out tests independently on each fibre without cracking it [14]. The tests were performed under controlled force with a constant loading rate of 1 mN/s. The stress-displacement curves were obtained by dividing the measured force during displacement by the section of the fibre being pushed. For each single-fibre push-out test, the stress σ_d corresponds to the initiation of the fibre-matrix debonding on the surface of the sample, resulting in the end of the linear domain of the elastic deformation of the fibre. For each test, the interfacial shear stress (ISS), τ , was determined using the following equation [15]:

$$\tau = \frac{F_p}{\pi D_f L_f}$$

where F_p is the plateau force at which the fibre is pushed out of the matrix after total debonding, D_f is the diameter of the tested fibre and L_f is its length (i.e. the specimen thickness).

Macro-mechanical tests

The macro-mechanical test specimens were laser cut (Trotec Speedy 400 Flexx - CO₂ Laser) from the as processed single-ply SiC/BN/SiC-Si composites. They were 30 mm long and 12 mm wide orientated within the fibre axis, and were about 0.5 mm thick. These samples, with four specimens for each plate, were cut perpendicularly to the major length for two reasons: (i) more specimens are available and (ii) unexpected bending is avoided. The tests were performed with an Instron 4505 electromechanical machine equipped with a 5 kN load cell, the crosshead speed being 0.05 mm/min.

On-axis tensile tests

Given the small dimensions of the specimens, aluminium extensions tabs of 14 mm × 40 mm were glued (3M Scotch-Weld EC-9323-2 B/A) to each end of the tensile specimens. Besides, it helped to fairly distribute the forces imposed by the jaws, the hydraulic pressure for jaw clamping being 20 bar. The strain was measured by two extensometers mounted on each opposite face of the specimen. The gauge length was 10 mm. From these tests, some sound values have been measured such as the initial Young's modulus within the fibre direction, E_1^0 , the pseudo elastic threshold $Rt_{0.005}$ and the maximum values of strain and stress reached during the test, ε_1^{\max} and σ_1^{\max} .

A pseudo-elastic threshold has been selected in place of the real damage threshold for the following reason: similarly to metallic alloy, the real threshold may be difficult to set up, especially when some damage (i.e. at least debonding) is present in the as-processed material. Different and quite numerous experiments at both Safran Ceramics and LCTS have led to choose the stress at a strain of 0.005 % (thus denominated $Rt_{0.005}$).

Besides, in order to remain in the homogeneous domain, i.e. before strain localization and the concomitant plateau or even the softening behaviour, maximum strain and stress values have been considered instead of their rupture values.

In-plane shear tests

A losipescu-type fixture was used for the in-plane shear tests. Because of the same small size of the specimens, aluminium extension tabs were added in two parts (14 × 40 mm² and 50 × 27 mm²) to fit the losipescu testing device, using the same glue.

The specimen strain fields between the end-tabs were monitored by digital image correlation (GOM-ARAMIS software) thanks to a speckle deposit.

Similarly to the tensile tests, values measured and reported elsewhere are the initial shear modulus G_{12}^0 , the pseudo-elastic threshold $Rs_{0.005}$ and the maximum values of angular shear strain (γ_6^{\max}) and shear stress (σ_6^{\max}) reached during the test.

Microscopy

Optical microscopy and scanning electron microscopy

A first field emission gun scanning electron microscope (FEG-SEM, Hitachi S4500 FEG) was used in the LCTS laboratory not only to measure the BN interphase thicknesses, but also to observe the fracture surface and the fibre pull-out of the composite specimens after the mechanical tests.

Cross-sections obtained from the mechanical specimens were also analysed. They were roughly 12 mm long and were located away from the fracture zone and from the end-tabs. After embedding in epoxy resin, the specimens were mirror polished (Buehler, MINIMET™ 1000). These sections were observed by optical microscopy (OM, Nikon ME600L) to obtain images which were analysed to calculate the proportions of the components and the area of the mechanically loaded section in each specimen. The matrix cracks were observed at the Centre de Microcaractérisation Raimond Castaing using a FIB FEG-SEM coupled with energy-dispersive spectroscopy (EDS). The apparatus used was a FEI Helios NanoLab 600i coupled to an Aztec Oxford EDS system (SDD detector, WD 4 mm). Cross sections of specific representative locations were obtained by focused ion beam (FIB) milling (Ga^+ ions). By alternating sequences of *in situ* FIB milling and SEM observation in a same sample area, matrix crack paths could be followed in all 3 spatial dimensions from the outside to the inside of tows.

Transmission electron microscopy

In a first step, small parts were taken from the samples of the composites after macro-mechanical testing. These epoxy-coated pieces were sandwiched between a silicon wafer and a glass slide and mechanically thinned to a thickness of 120 μm . The electronic transparency was obtained in a second step by ion milling using two different methods. The first method was carried out at LCTS, based on the milling of the sample by a low-energy Ar^+ ion beam (JEOL, Ion Slicer, EM-09100IS). The second method was carried out at the Centre de Microcaractérisation Raimond Castaing by FIB milling.

The thin foils thus prepared were then observed by transmission electron microscopy (TEM, Philips, CM30ST, the LaB_6 source operating at 300 kV). Direct images in both bright field (BF) and dark field (DF) modes were recorded. The DF images were formed from electron beams scattered by sp^2 -BN basal atomic layers of 0.33 nm spacing. High-resolution transmission electron microscopy (HRTEM) images were obtained in the thinnest areas of the thin foils. Selected area electron diffraction (SAED) patterns were recorded from areas of 400 nm in diameter within thick interphases.

Results

Fibre push-out behaviour

On Fig. 1 are displayed typical push-out test curves obtained from single-fibres selected from the single-ply SiC/BN/SiC-Si composites with the different BN interphases. The values of the interfacial micromechanical characteristics deduced from all these push-out curves are reported in Table 2.

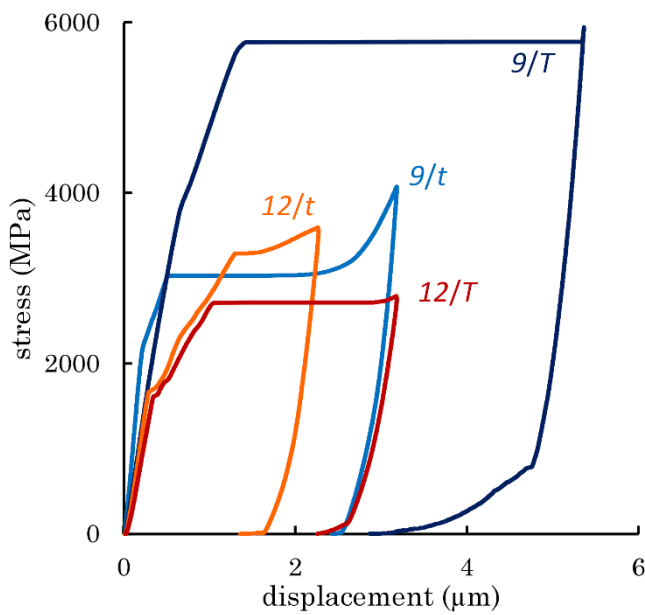


Fig. 1 Typical single-fibre push-out curves for the single-ply composites with the 4 different BN interphases

It may be seen that the values of τ and σ_d clearly depend on the crystallization degrees and the thicknesses of the BN interphases. Besides, whatever the thickness, the ISS values are higher with the interphases prepared at 900 °C than with those prepared at 1200 °C.

For the interphases prepared at 900 °C, the best fibre-matrix interfacial bonding is obtained with a target thickness of 500 nm for which τ reaches an average value of 124 ± 9 MPa. These ISS values are higher than those measured in SiC/BN/SiC composites by Morscher *et al.* by push-in tests with Sylramic-iBN fibres (~ 80 MPa) [25] or more recently by push-out tests with Hi-Nicalon fibres by Gavalda-Diaz *et al.* [26, 27] and with Hi-Nicalon type S fibres by De Meyere *et al.* (~ 30 MPa) [14]. Rebillat *et al.* obtained ISS values of about 140 MPa by push-out tests on microcomposites with treated Nicalon fibres and a special BN interphase leading to a "strong interface" [28]. Thus, providing that its thickness is sufficient, the poorly crystallised BN interphase of the present work results in a fibre-matrix bonding that can also be qualified as strong. It should be noted that even higher values were found by Le Gallet *et al.* and Jacques *et al.* in minicomposites with BN interphases and Hi-Nicalon fibres (up to

~220-230 MPa). Yet, these values were estimated from tensile tests performed at the macro-scale [13] [29].

For the interphases prepared at 1200 °C, τ values are low and similar for the two thicknesses tested, around 35-40 MPa. The fibre-matrix interfacial bonding can thus be qualified as weak when the interphases have a high crystallisation degree.

Table 2 Mechanical results

		interphase	9/t	9/T	12/t	12/T	
micromechanics	(push-out)	σ_d	mean (MPa)	2101	3996	1446	1223
			standard deviation (MPa)	300	456	548	368
			number of tests	17	16	25	12
		τ	mean (MPa)	74	124	41	34
			standard deviation (MPa)	14	9	6	12
			number of tests	19	15	14	15
macro-mechanical properties	on-axis tensile tests	E_1^0	mean (GPa)	261	250	165	229
			standard deviation (GPa)	34	33	18	27
			number of specimens	7	8	4	6
		$Rt_{0.005}$	mean (MPa)	194	161	92	137
			standard deviation (MPa)	28	41	15	24
			number of specimens	7	7	4	7
		ε_1^{\max}	mean (%)	0.33	0.46	0.28	0.28
			standard deviation (%)	0.08	0.09	0.1	0.05
			number of specimens	7	7	4	7
		σ_1^{\max}	mean (MPa)	336	350	158	306
			standard deviation (MPa)	34	39	10	43
			number of specimens	7	7	4	7
in-plane shear tests	G_{12}^0	mean (GPa)	86	76	61	60	
		standard deviation (GPa)	23	12	6	9	
		number of specimens	4	4	4	4	
	$Rs_{0.005}$	mean (MPa)	78	78	37	61	
		standard deviation (MPa)	29	16	1	10	
		number of specimens	4	4	4	4	
	γ_6^{\max}	mean (%)	0.32	0.5	0.33	0.3	
		standard deviation (%)	0.07	0.15	0.01	0.05	
	number of specimens	4	4	2	4		
	σ_6^{\max}	mean (MPa)	145	123	85	120	
		standard deviation (MPa)	31	11	2	13	
		number of specimens	4	4	2	4	

On-axis tensile behaviour

Regarding the mechanical behaviour of the model composites at the macro-scale, Fig. 2 shows examples of tensile stress-strain curves obtained with the 4 composites possessing different BN interphases. The nonlinear curves are typical of CMCs with non-brittle behaviours involving multi-cracking of the matrix as well as concomitant fibre-matrix debonding. The values of E_1^0 , $Rt_{0.005}$, ϵ_1^{\max} , and σ_6^{\max} deduced from all the tensile curves are presented in Table 2. The lowest tensile mechanical properties are obtained for 12/t whereas the best maximum properties are obtained with the 9/T interphase. However, if the average maximum strain is clearly higher with this interphase, the mechanical strength is on the other hand close to those obtained with the other two interphases: 9/t and 12/T.

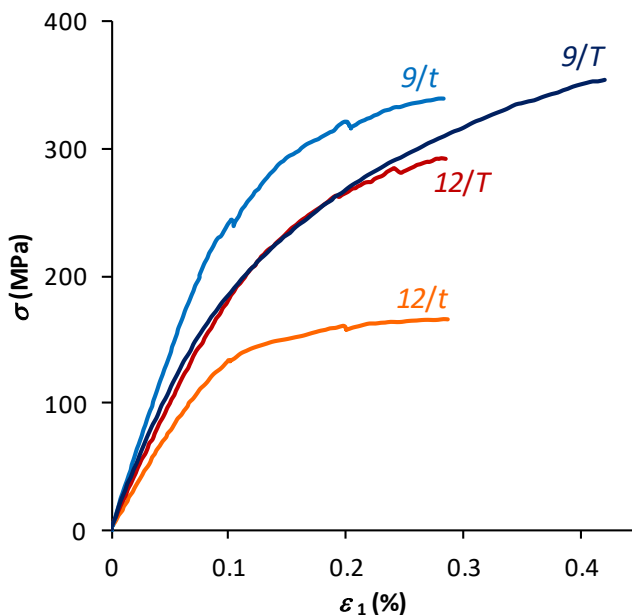


Fig. 2 Examples of monotonic stress/strain curves obtained in on-axis tension for the 4 different SiC/BN/SiC-Si composites

On-axis in-plane shear behaviour

The matrix fracture surfaces observed after the on-axis in-plane shear tests are oriented at 45° to the fibres (Fig. 3). This feature is typical for tests involving shear loading of the fibre-matrix interfaces in CMCs possessing a stiff matrix [30, 31]. The fibre pull-outs show that the BN interphases do act as a mechanical fuse. The average curves of in-plane shear stress versus angular shear strain are presented in Fig. 4. As in the tensile tests, the shape of the curves is typical of the behaviour of CMCs, with a nonlinear domain linked to microcracking and fibre-matrix debonding following the initial linear elastic

region. Each curve is based on 4 tests for each type of interphase, except for the $12/t$ interphases where only half of the tests were fully valid. However, all initial plane shear moduli deduced from the linear domains appear to be well representative of the materials and were therefore accounted for. The average values of G_{12}^0 , $R_{s_{0.005}}$, γ_6^{\max} and σ_6^{\max} deduced from the tests are reported in Table 2.

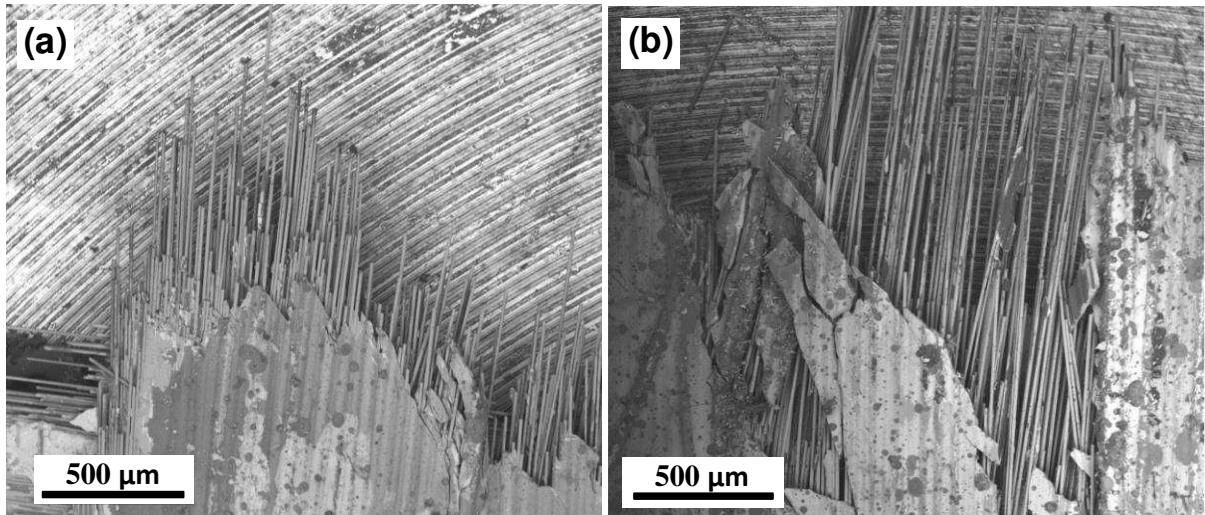


Fig. 3 Rupture surface obtained from SEM observations on samples tested in shear with (a) an interphase $9/t$ and (b) $12/T$

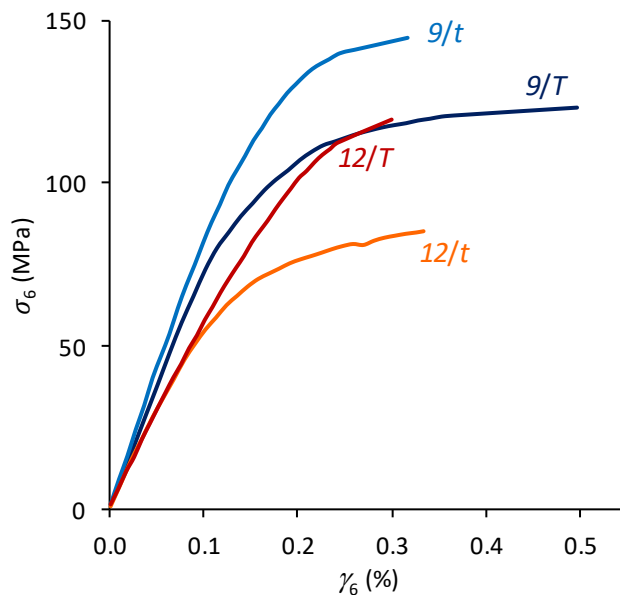


Fig. 4 Monotonic shear curves of the 4 different SiC/BN/SiC-Si composites

The conclusions that can be drawn from these in-plane shear tests are roughly similar to those derived from tensile tests. The average mechanical properties obtained with the interphases synthesised at

900 °C are better than those obtained with the interphases synthesised at 1200 °C. In particular, the composites are stiffer ($G_{12}^0(9/) \approx 80$ GPa vs. $G_{12}^0(12/) \approx 60$ GPa) and the apparent onset of the first cracks takes place later with the interphases synthesised at 900 °C than with the interphases synthesised at 1200 °C ($Rs_{0.005}(9/) \approx 80$ MPa vs. $Rs_{0.005}(12/) \approx 40-60$ MPa).

For a given temperature of interphase synthesis, the thickness of the interphase influences the in-plane shear maximum homogeneous properties of the CMCs. For the interphases synthesised at 900 °C, the thickness of 500 nm results in maximum angular strains of $\sim 0.5\%$. However, the best mechanical shear strength is obtained with the thickness of 200 nm ($\sigma_6^{\max} = 145 \pm 31$ MPa). For the interphases synthesised at 1200 °C, the average mechanical shear strength is better with the 500 nm thick interphase than with the 200 nm thick interphase ($\sigma_6^{\max} = 120 \pm 13$ MPa and $\sigma_6^{\max} = 85 \pm 2$ MPa respectively), almost at the level of the best BN900 interphases if scattering is considered.

Crack morphologies after in-plane shear tests

If the mechanical behaviour of a CMC cannot be quantified from its crack morphology alone, multiple observations of CMCs with different properties after mechanical tests allow however comparisons and identifications of trends. That is what motivates the search for results obtained from these observations. As sound results were better obtained with in-plane shear tests, observations of crack morphologies were focused on samples obtained from these tests.

Meso-scale

For the poorly crystallised interphases prepared at 900 °C, the matrix cracks show different morphologies depending on their thickness. When this thickness is about 200 nm, the crack is open, with an opening of a few micrometres (Fig. 5a). It splits and propagates over long distances inside the tows. When the interphase thickness is 500 nm, the matrix cracks are thinner (less than one micron of opening), does not split, and propagates over short distances within a tow (Fig. 5b).

When considering the highly crystallised interphases prepared at 1200 °C the matrix crack morphologies are similar. For both the 200 nm and 500 nm thicknesses, the cracks are few in number, wide open (approaching ten microns) and tend to split. They propagate both between and within the tows over very long distances. An example of this feature is given in Fig. 5c for the 12/t interphase.

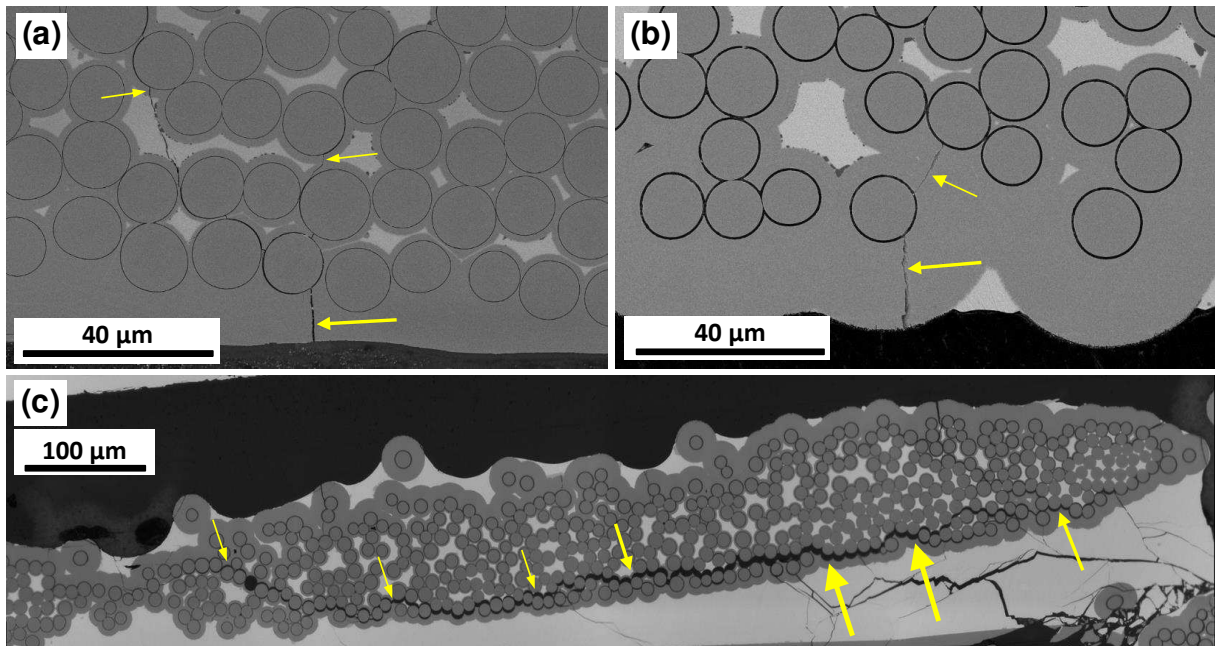


Fig. 5 SEM observations of cracks induced by a shear loading on single-ply 2D SiC/SiC-Si composites with various interphases, (a) 9/t, (b) 9/T and (c) 12/t

Micro-scale

In the case of the interphase synthesised at 900 °C and with a thickness of 200 nm, the main crack observed by SEM on the FIB cross-sections has a large opening of about 0.3 μm (Fig. 6a). EDS analyses revealed the presence of carbon and oxygen in the crack on the sample surface, certainly due to the infiltration of the resin used to prepare the section. The vertical straight stripes visible on the milled surfaces in the micrographs are artefacts resulting from a curtaining effect of the ion mill. As the FIB milling proceeded, the main crack was accompanied by small, thin secondary cracks with an opening of less than twenty nanometres. Eventually, only the secondary cracks remained.

Tracking of a secondary crack is possible due to the resin leading to the formation of small bulges, pores and edgings that are visible by SEM. For example, Fig. 6b shows the deflection of a secondary matrix crack in a rare case where a thin fibre-matrix debonding occurred in the interphase on the matrix side (unmeasurable opening). However, with the 9/t interphase, the majority of debonds have a large opening (up to ~150 nm) and occur on the fibre side (Fig. 7) according to the mechanism termed “inside” debonding by Morscher *et al.* [25].

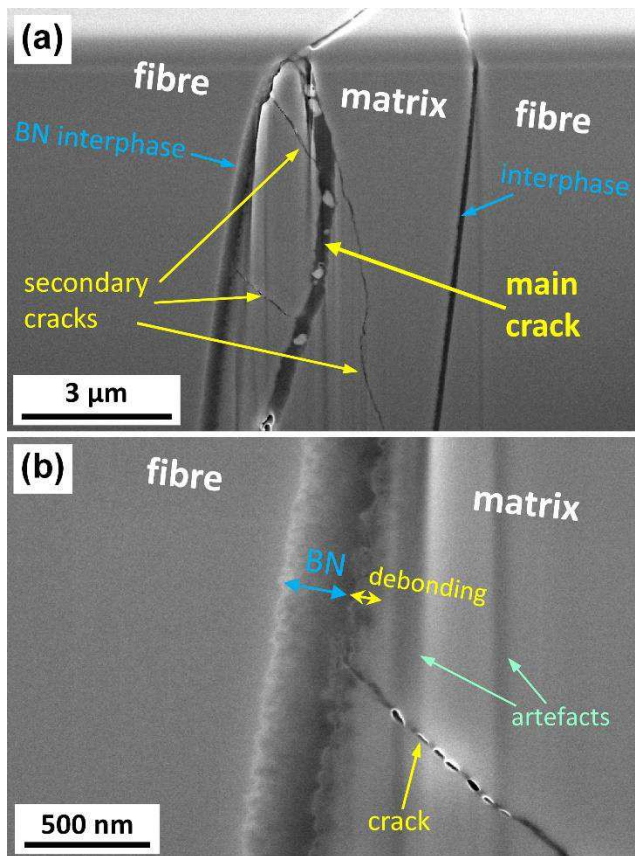


Fig. 6 FIB-SEM images of a crack in a single-ply composite with a $9/t$ interphase of a sample tested in shear. **(b)** is a magnification of **(a)**

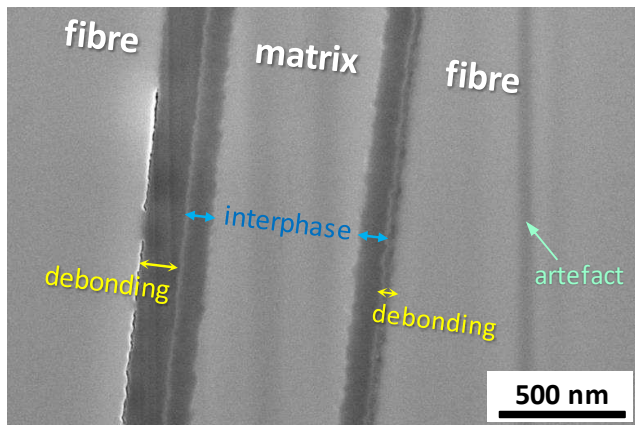


Fig. 7 FIB-SEM image of interfacial debonding a single-ply composite with a $9/t$ interphase

Numerous cracks and debonds could be observed in the thin foil prepared conventionally in the LCTS laboratory from a sample tested in shear with the $9/t$ interphase. Matrix crack deflections and wide debonding (up to 300 nm in opening) can occur in the middle of the interphase or on the matrix side. However, inside debonding (along the surface of the fibre) is most often observed (Fig. 8a). HR-MET

observation shows that a few basal atomic planes of sp^2 -BN remain attached to the fibre (Fig. 8b). While at a larger scale of observation the interphase failure may appear adhesive, at this very small scale it can be called to be in fact "cohesive near the interface". It can be assumed that these atomic planes, which are locally better organised than in the rest of the interphase [20], remain a weak link in the interphase.

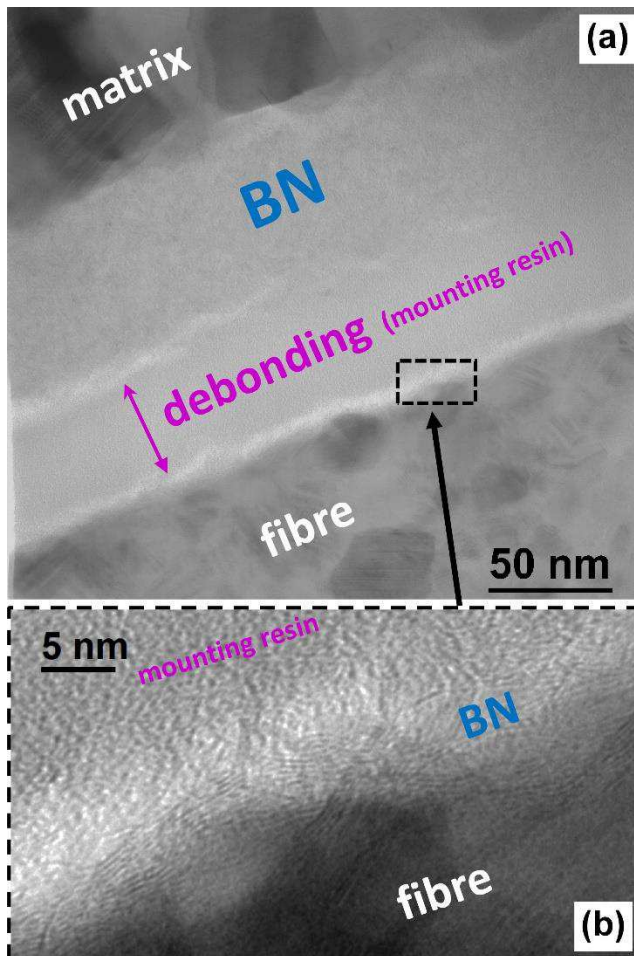


Fig. 8 HR-TEM observation of debonding in a 9/t interphase after in-plane shear test, (b) is a detail of (a)

In the case of an interphase also synthesised at 900 °C but with a thickness of 500 nm, the matrix cracks found on the surface are thin and remain thin without undergoing splitting into secondary cracks in the section after FIB milling. Although the opening width could not be measured, crack tracking was facilitated by an edge brightness effect. The deflection from mode I to mode II occurs gradually in the interphase from the matrix side to the fibre side where the crack seems to stop its propagation (Fig. 9a). Deeper into the FIB milling section, deflections of the same matrix crack can be observed in the interphases of two adjacent fibres (the crack branches in the interphases as it deflects). (Fig. 9b).

The debonds between fibres and matrix are not clearly visible. But since the crack seems to reach the surface of the fibres through the interphase without causing their failure, it can be assumed that the debonds are very thin and take place on the surface of the fibres.

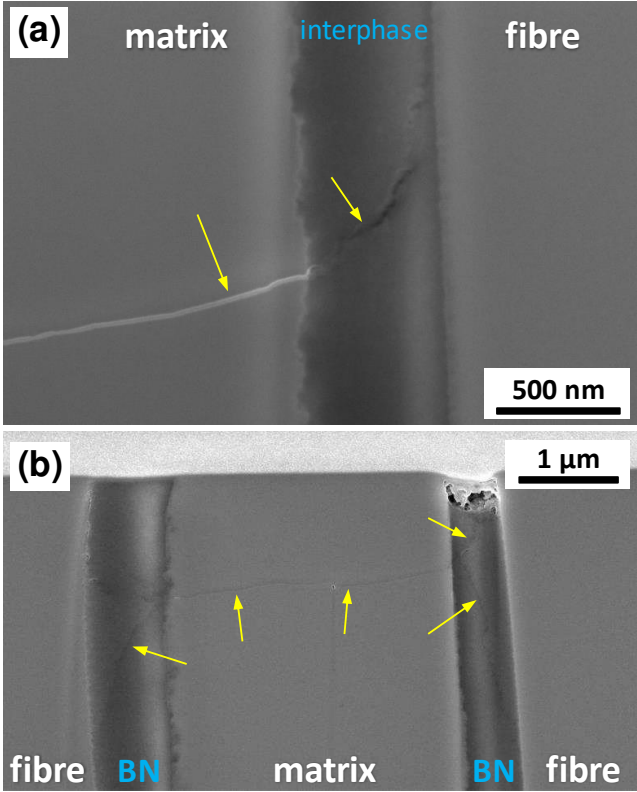


Fig. 9 FIB-SEM images of a crack (yellow arrows) in a single-ply sample with a 9/T interphase. (b) is further in the cutting than (a)

Cracks and debonds with a 9/T interphase could only be observed by TEM in a thin specimen prepared by FIB at the Centre de Microcaractérisation Raimond Castaing. One of these observable debonds is presented in Fig. 10. It is thin and does take place on the fibre side.

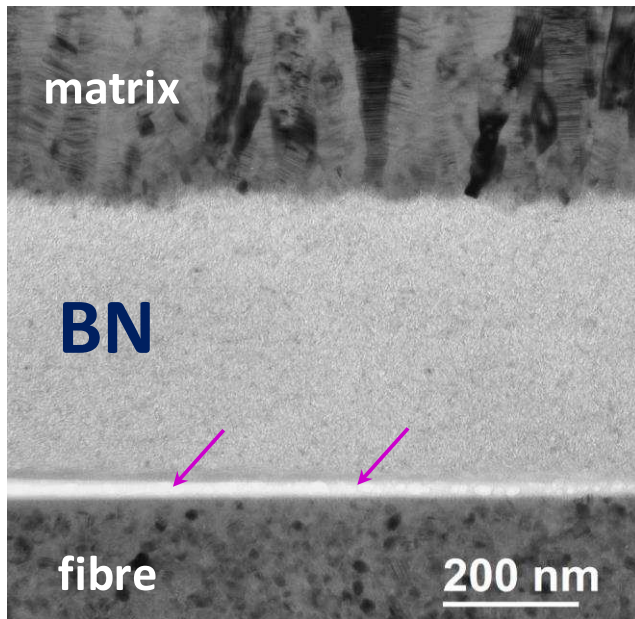


Fig. 10 BF-TEM observation of a debond (purple arrows) in a $9/T$ interphase after in-plane shear test

In the case of interphases synthesised at 1200 °C, either with a target thickness of 200 nm or with one of 500 nm, the cracks are very open ($\sim 0.3 \mu\text{m}$) (Fig. 11). The main crack is accompanied by secondary cracks (not always visible on the surface), forming a network of intersecting cracks. As in the former cases, EDS analysis indicates that these cracks are filled with resin. Deeper into the milled sections, very open main and secondary cracks still take place. For both interphase thicknesses, very open debonding occurs either at the fibre-interphase interface or at the interphase-matrix interface. Fig. 12 shows an example of a crack deflection with debonding on the matrix side.

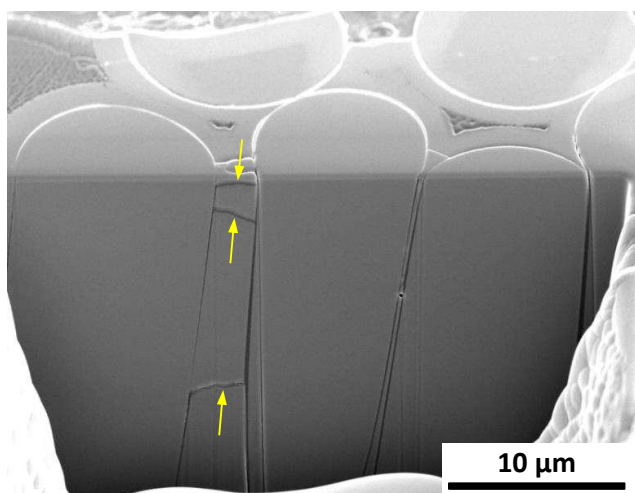


Fig. 11 FIB-SEM image of cracks in a SiC/BN/SiC-Si single-ply sample with a $12/t$ interphase

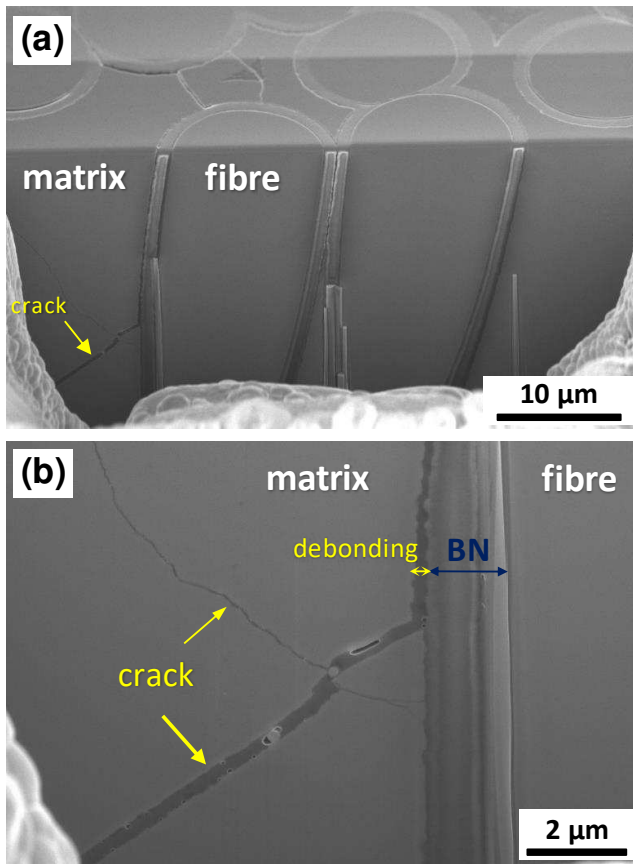


Fig. 12 FIB-SEM image of cracks in a SiC/BN/SiC-Si single-ply sample with a 12/T interphase after a shear test. **(b)** is a magnification of **(a)**

TEM observations show debonds within the interphases with no preferred location (Fig. 13). No obvious debonds are observed at the interfaces with both the fibre and the matrix. It can be noted that the interphases can be either thinner than expected as in Figs. 13a (without taking the debonding into account) and 13c or thicker than expected as in Fig. 13b. This heterogeneity in thickness may indicate a difficulty in infiltrating the BN interphases at 1200 °C.

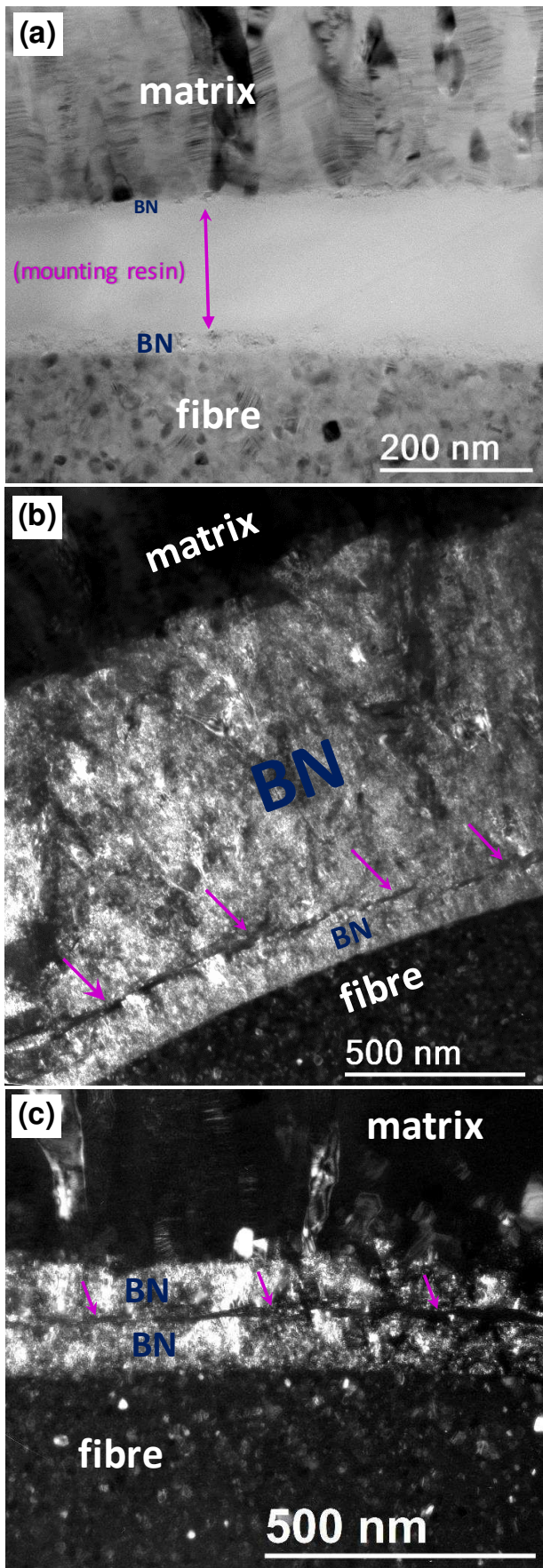










Fig. 13 TEM observations of debonds (purple arrows) (a) in BF mode in an interphase $12/t$, and (b) and (c) in DF mode in interphases $12/T$ after in-plane shear test

A summary of all these micro-scale observations describing crack morphologies and debonds is presented in Table 3.

Table 3 Summary table of the morphological observations performed on the 4 different single-ply SiC/BN/SiC-Si composites regarding cracks and debonds

	interphase	9/t	9/T	12/t and 12/T
OM	opening			
	splitting	+	∅	+
	length	—	-	—
	inter-tow	∅	∅	+
	intra-tow	+	+	+
FIB-SEM	opening			
	splitting	+	∅	+
	BN/M	~∅	∅	+
	F/BN	++	++	+
	BN	∅	∅	+
TEM	opening			 and
	BN/M	+	∅	+
	F/BN	++	+	+
	BN	+	∅	+

crack opening: : very wide, : wide, |: small

crack length: —: long, -: short

++: very frequent, +: frequent, ~∅: rare, ∅: absent

BN/M, F/BN, BN: location of debonding on the fibre side, on the matrix side or in the middle of the interphase respectively.

Discussion

The scattering observed with the macro-mechanical tests is typical of CMCs and is of the same level for each type of interphase. Taking this scattering into account, it appears that the thinnest interphase synthesised at 1200 °C leads to significantly poorer macro-mechanical properties than for the other three interphases. It should be noted that for these three other interphases, the differences that may appear between the average macro-mechanical characteristics are in agreement with the results of the micromechanical tests. However, these differences are quite tenuous, which hardly allows

discerning the roles of these interphases on the behaviour of the single-ply composites. On the other hand, the effects of the microstructure of the BN interphases and of the thickness for the weakly organised interphase are clearly visible in push-out and in terms of crack morphology.

Push-out obtained ISS values show that the thickness of the interphases synthesised at 1200 °C has little effect on these values. Yet, scattering of the results is proportionally higher for 12/*T* than with the other interphases. This scattering may be related to the high deposition rate of BN at high temperature which, even in a single-ply composite *a priori* simpler to infiltrate than an industrial composite, leads to infiltration issues, i.e. strong interphase thickness gradients and therefore heterogeneity as shown in TEM (Fig. 13). Compared to 12/*t*, increasing the thickness of this interphase by increasing the processing duration allows more time for the gaseous precursors to infiltrate the tows and thus leads to fewer fibres being poorly coated. In addition, it creates r-BN crystallites which increase the surface roughness of the interphase [20], and can then promote interlocking of the matrix with the interphase. Although these effects are not evidenced in micromechanics, it however results in better macro-mechanical properties. It seems that obtaining a BN interphase with a high degree of crystallisation while having a homogeneous thickness throughout the fibre preform would further improve the behaviour of these SiC/BN/SiC-Si composites. One way to achieve this would be to use a continuous CVD process [32, 33]. Such a process in which a single tow is treated separately reduces the infiltration gradients and coats the fibres homogeneously. The tow thus prepared must then be shaped (braiding, weaving...) to elaborate the preform and manufacture the final CMC.

Whatever the interphase thickness, $\alpha(9/)$ is greater than $\alpha(12/)$. This was anticipated by Gavalda-Diaz *et al.* [27]. A low degree of crystallisation of isotropic t-BN classically infiltrated at low temperature is related to local atomic stacking defects which increase the bonding between the sp²-BN basal planes. Conversely, in the case of a 12/ interphase deposited at high temperature, the sp² hybridisation nature of t-BN is more pronounced with basal planes preferentially aligned parallel to the fibre. Because of the weak bonding between these planes, the ratio of the critical energy release rate in the deflection direction towards the one in the propagation direction G_c^d/G_c^p is likely reduced. The cohesive character of the failure is consequently reinforced as revealed by microscopic observations: the preferential place of debonding shifts away from the surface of the fibre.

By contrast, in the case of 9/ interphases synthesised at 900 °C, the decrease in ISS with the decrease of the interphase thickness found here is counterintuitive and has no obvious explanation. It contradicts, for example, the fibre push-out results obtained by De Meyere *et al.* with their HNS/BN/SiC CMCs [14]. The number of tests performed is much smaller and therefore the statistical study is far from being as sound as that of De Meyer *et al.* It should be noted, however, that with 9/ interphases our ISS values are globally higher than theirs, probably due to the initial fibre surface treatment. The

resulting strengthening of the interfacial bonding could be the reason for a different effect of the interphase thickness.

The crack morphologies are in good agreement with the macro-mechanical and moreover the micro-mechanical properties: a stronger fibre-matrix bond (high σ_a and τ) means higher tensile and shear strengths, as well as shorter and thinner cracks. Compared to micro- and minicomposites, the use of single-ply composites as model specimens to study interphases is particularly relevant here, and their synthesis remains sufficiently easy at the laboratory scale.

The openings and lengths of cracks, which can occur for example in an accidental situation with a CMC, are important characteristics to control. Indeed, even if they seem to have little influence on the overall macro-mechanical behaviour, strong bonds reduce these cracks, thus confining the gap left for corrosive species which could enter them. Beyond the organisation of BN and the exact location of preferential debonding in the interphase, it is mostly the confinement and the synergy between BN and SiC that allow the easy formation of borosilicate seals protecting the BN interphase from corrosion [34, 35]. Thus, for the synthesis of a BN interphase using the CVI batch process, it is advantageous to favour conditions that give a sufficiently thick but submicron coating with a low degree of crystallisation to obtain a strong fibre-matrix bond.

There is still room for improving the behaviour of SiC/SiC composites with BN CVI interphases. The presence of small defects or pores at the BN-fibre interface was not observed as in the work of Gavalda-Diaz *et al.* carried out with untreated Hi-Nicalon fibres [27]. In the present work, the failures are nevertheless close to the interface with the fibre but they are cohesive at the nanoscale, and ISS values above 100 MPa could be obtained. While inside debonding is not *a priori* a concern, it appears to be due to the preferential alignment of the first sp^2 -BN atomic planes. Preventing this local organisation through a better control of the deposition transient would further increase the bonding to the fibre.

Conclusion

A hierarchy of fibre-matrix bonding strengths as a function of the thickness and degree of crystallisation of the BN interphase could be established using single-ply model SiC/BN/SiC-Si composites. The observations made at different scales are consistent with each other and, besides, also with microscopic and macroscopic behaviours. Depending on the interphases, the main matrix cracks are more or less long and open, leading or not to secondary cracking. Besides, debonds are more or less pronounced and occur preferentially at different locations in the interfacial system.

A low crystallisation degree of a BN interphase synthesised at 900 °C always leads to a stronger fibre-matrix bond and a better mechanical behaviour of the resulting CMC than a high degree of crystallisation interphase synthesised at 1200 °C. For this kind of interphase synthesised at 900 °C, a thickness of 500 nm is preferable to a thickness of 200 nm.

It would now be worth studying the macroscopic mechanical behaviour under high temperature oxidising environments of these single-ply composites to verify that the BN interphase g/T , which is considered to be the most interesting, will still be interesting under the conditions of the aimed application.

Ethics declarations

Conflict of interest

Author H. Delpouve has received a PhD grant from SAFRAN CERAMICS.

References

- [1] Kellner T (2016) Space age ceramics are aviation's new cup of tea. GE Int. <https://www.ge.com/news/reports/space-age-cmcs-aviations-new-cup-of-tea>. Accessed 14 June 2022
- [2] Bouillon E, Laval N, Marsal D (2017) SiC-based ceramic matrix composite behavior enhancement for gas turbines hot sections. In: Kagawa Y, Zhu D, Darolia R, Raj R (eds) Advanced Ceramic Matrix Composites: Science and Technology of Materials, Design, Applications, Performance and Integration, ECI Symposium Series. <https://dc.engconfintl.org/acmc/47>
- [3] DiCarlo JA (2014) Advances in SiC/SiC composites for aero-propulsion. In: Bansal NP, Lamon J (eds) Ceramic Matrix Composites: Materials, Modelling and Technology, John Wiley & Sons, Inc., Hoboken, NJ, USA, pp. 217-235 <https://doi.org/10.1002/9781118832998.ch7>
- [4] Liu QM, Huang SZ, He AJ (2019) Application requirements and challenges of CMC-SiC composites on aero-engine. J Mater Eng 47:1-10 <https://doi.org/10.11868/j.issn.1001-4381.2018.000979>
- [5] Wang X, Gao X, Zhang Z, Cheng L, Ma H, Yang W (2021) Advances in modifications and high-temperature applications of silicon carbide ceramic matrix composites in aerospace: A focused review. J Eur Ceram Soc 41:4671–4688 <https://doi.org/10.1016/j.jeurceramsoc.2021.03.051>

- [6] Naslain RR, Paillet RJF, Lamon JL (2010) Single- and multilayered interphases in SiC/SiC composites exposed to severe environmental conditions: an overview. *Int J Appl Ceram Technol* 7:263–275 <https://doi.org/10.1111/j.1744-7402.2009.02424.x>
- [7] Chawla KK (1993) Interface mechanics and toughness. In: *Ceramic Matrix Composites*. Springer, Boston, MA. https://doi.org/10.1007/978-1-4757-2216-1_9
- [8] Miller JH, Lowden RA, Liaw PK (1994) Fiber coatings and the fracture behavior of a continuous fiber ceramic composite. *Mat Res Soc Symp Proc*, 365:403–410 <https://doi.org/10.1557/PROC-365-403>
- [9] Sauder C, Brusson A, Lamon J (2010) Influence of interface characteristics on the mechanical properties of Hi-Nicalon type-S or Tyranno-SA3 fiber-reinforced SiC/SiC minicomposites. *Int J Appl Ceram Technol* 7:291–303 <https://doi.org/10.1111/j.1744-7402.2010.02485.x>
- [10] Karakoc O, Koyanagi T, Nozawa T, Katoh Y (2021) Fiber/matrix debonding evaluation of SiC_f/SiC composites using micropillar compression technique. *Compos B Eng* 224:109189 <https://doi.org/10.1016/j.compositesb.2021.109189>
- [11] Buet E, Braun J, Sauder C (2022) Influence of texture and thickness of pyrocarbon coatings as interphase on the mechanical behavior of specific 2.5D SiC/SiC composites reinforced with Hi-Nicalon S fibers. *Coatings* 12:573 <https://doi.org/10.3390/coatings12050573>
- [12] Prouhet S, Camus G, Labrugere G, Guette A, Martin E (1994) Mechanical characterization of Si–C(O) fiber/SiC (CVI) matrix composites with a BN–Interphase. *J Am Ceram Soc* 77:649–656 <https://doi.org/10.1111/j.1151-2916.1994.tb05344.x>
- [13] Le Gallet S, Rebillat F, Guette A, Bourrat X, Doux F (2004) Influence of a multilayered matrix on the lifetime of SiC/BN/SiC minicomposites. *J Mater Sci* 39:2089–2097 <https://doi.org/10.1023/B:JMSC.0000017771.93067.42>
- [14] De Meyere RMG, Gale L, Harris S, Edmonds IM, Marrow TJ, Armstrong DEJ (2021) Optimizing the fiber push-out method to evaluate interfacial failure in SiC/BN/SiC ceramic matrix composites. *J Am Ceram Soc* 104:2741–2752 <https://doi.org/10.1111/jace.17673>
- [15] Rebillat F, Lamon J, Naslain R, Lara-Curzio E, Ferber MK, Besmann TM (1998) Interfacial bond strength in SiC/C/SiC composite materials, as studied by single-fiber push-out tests. *J Am Ceram Soc* 81:965–978 <https://doi.org/10.1111/j.1151-2916.1998.tb02434.x>
- [16] Lv X, Yue M, Yang W, Feng X, Li X, Wang Y, Wang J, Zhang J, Wang J (2021) Tunable strength of SiC_f/β-Yb₂Si₂O₇ interface for different requirements in SiC_f/SiC CMC: Inspiration from model

- composite investigation. *J Mater Sci Technol* 67:165–173
<https://doi.org/10.1016/j.jmst.2020.05.071>
- [17] Lu Z, Yue J, Fu Z, Huang X, Yang H (2020) Microstructure and mechanical performance of SiC_f/BN/SiC mini-composites oxidized at elevated temperature from ambient temperature to 1500 °C in air. *J Eur Ceram Soc* 40:2821–2827
<https://doi.org/10.1016/j.jeurceramsoc.2019.04.013>
- [18] Naslain R (2004) Design, preparation and properties of non-oxide CMCs for application in engines and nuclear reactors: an overview. *Compos Sci Technol* 64:155–170
[https://doi.org/10.1016/S0266-3538\(03\)00230-6](https://doi.org/10.1016/S0266-3538(03)00230-6)
- [19] Carminati P, Buffeteau T, Daugey N, Chollon G, Rebillat F, Jacques S (2018) Low pressure chemical vapour deposition of BN: Relationship between gas phase chemistry and coating microstructure. *Thin Solid Films* 664:106–114 <https://doi.org/10.1016/j.tsf.2018.08.020>
- [20] Plaisantin H, Jacques S, Danet J, Camus G, Delpouve H (2021) TEM characterization of turbostratic and rhombohedral BN interphases synthesized by chemical vapour infiltration in SiC/SiC-Si composites. *Mater Charact* 172:110857
<https://doi.org/10.1016/j.matchar.2020.110857>
- [21] Naslain R, Lamon J, Paillet R, Bourrat X, Guette A, Langlais F (1999) Micro/minicomposites: a useful approach to the design and development of non-oxide CMCs. *Compos Part A Appl Sci Manuf* 30:537–547 [https://doi.org/10.1016/S1359-835X\(98\)00147-X](https://doi.org/10.1016/S1359-835X(98)00147-X)
- [22] Swaminathan B, McCarthy NR, Almansour AS, Sevenser K, Pollock TM, Kiser JD, Daly S (2021) Microscale characterization of damage accumulation in CMCs. *J Eur Ceram Soc* 41:3082–3093
<https://doi.org/10.1016/j.jeurceramsoc.2020.05.077>
- [23] Loison S, Huguet C, Delcamp A, Buet E (2016) Silicon carbide fiber treatment method. Patent WO2016207534 International Application No. PCT/FR2016/051508
- [24] Rebillat F, Lamon J, Naslain R, Lara-Curzio E, Ferber MK, Besmann TM (1998) Properties of multilayered interphases in SiC/SiC chemical-vapor-infiltrated composites with “weak” and “strong” interfaces. *J Am Ceram Soc* 81:2315–2326 <https://doi.org/10.1111/j.1151-2916.1998.tb02627.x>
- [25] Morscher GN, Yun HM, DiCarlo JA, Thomas-Ogubui L (2004) Effect of a boron nitride interphase that debonds between the interphase and the matrix in SiC/SiC composites. *J Am Ceram Soc* 87:104–112 <https://doi.org/10.1111/j.1551-2916.2004.00104.x>

- [26] Gavalda-Diaz O, Marquardt K, Harris S, Gale L, Vandeperre L, Saiz E, Giuliani F (2020) Degradation mechanisms of SiC/BN/SiC after low temperature humidity exposure. *J Eur Ceram Soc* 40:3863–3874 <https://doi.org/10.1016/j.jeurceramsoc.2020.05.007>
- [27] Gavalda-Diaz O, Manno R, Melro A, Allegri G, Hallett SR, Vandeperre L, Saiz E, Giuliani F (2021) Mode I and Mode II interfacial fracture energy of SiC/BN/SiC CMCs. *Acta Mater* 215:117125 <https://doi.org/10.1016/j.actamat.2021.117125>
- [28] Rebillat F, Lamon J, Guette A (2000) The concept of a strong interface applied to SiC/SiC composites with a BN interphase. *Acta Mater* 48:4609–4618 [https://doi.org/10.1016/S1359-6454\(00\)00247-0](https://doi.org/10.1016/S1359-6454(00)00247-0)
- [29] Jacques S, Bonnetot B, Berthet MP, Vincent H (2004) BN interphase processed by LP-CVD from tris(dimethylamino)borane and characterized using SiC/SiC minicomposites. *Ceram Eng Sci Proc* 25:123-128 <http://dx.doi.org/10.1002/9780470291191.ch20>
- [30] Lynch CS, Evans AG (1996) Effects of off-axis loading on the tensile behavior of a ceramic-matrix composite. *J Am Ceram Soc* 79:3113-3123 <https://doi.org/10.1111/j.1151-2916.1996.tb08085.x>
- [31] Camus G (2000) Modelling of the mechanical behavior and damage processes of fibrous ceramic matrix composites: application to a 2-D SiC/SiC. *Int J Solids Struct* 37:919-942 [http://dx.doi.org/10.1016/S0020-7683\(99\)00065-7](http://dx.doi.org/10.1016/S0020-7683(99)00065-7)
- [32] Jacques S, Vincent C, Vincent H, Lopez-Marure A, Bouix J (2001) Multilayered BN coatings processed by a continuous LPCVD-treatment onto Hi-Nicalon fibers. *J Solid State Chem* 162:358-363 <http://dx.doi.org/10.1006/jssc.2001.9387>
- [33] Suzuki M, Tanaki Y, Inoue Y, Miyamoto N, Sato M, Goda K (2003) Uniformization of boron nitride coating thickness by continuous chemical vapor deposition process for interphase of SiC/SiC composites” *J Ceram Soc Jpn* 111:865-871 <https://doi.org/10.2109/jcersj.111.865>
- [34] Yang H, Lu Z, Bie B, Fu Z, Yue J, Huang X (2019) Microstructure and damage evolution of SiC_f/PyC/SiC and SiC_f/BN/SiC mini-composites: A synchrotron X-ray computed microtomography study. *Ceram Int* 45:11395–11402 <https://doi.org/10.1016/j.ceramint.2019.03.004>
- [35] Carminati P, Jacques S, Rebillat F (2021) Oxidation/corrosion of BN-based coatings as prospective interphases for SiC/SiC composites. *J Eur Ceram Soc* 41:3120–3131 <https://doi.org/10.1016/j.jeurceramsoc.2020.07.056>